electronics

MDPI

Article

Zero-Power Control Strategy and Dynamics Enhancement for Hybrid Maglev Conveyor Cart

Xiaowei Tang [1,2], Seiji Hashimoto [2,*], Takahiro Kawaguchi [2] and Nobuyuki Kurita [2]

[1] College of Intelligent Manufacturing, Yangzhou Polytechnic Institute, Yangzhou 225127, China; t222d005@gunma-u.ac.jp
[2] Division of Electronics and Informatics, School of Science and Technology, Gunma University, 1-5-1 Tenjin-cho, Kiryu 376-8515, Japan; kawaguchi@gunma-u.ac.jp (T.K.); nkurita@gunma-u.ac.jp (N.K.)
* Correspondence: hashimotos@gunma-u.ac.jp; Tel.: +81-277-30-1741

Abstract: This paper presents a novel zero-power controller applied to a four-unit magnetic levitation system, aimed at addressing the challenge of maintaining stability under disturbance loads. The zero-power controller, designed based on a state feedback controller integrated with a position servo integrator, is primarily employed to control the balance of the magnetic levitation (Maglev) unit and eliminate steady-state errors. Subsequently, the zero-power controller operates after the state feedback controller to adjust the Maglev unit to a new equilibrium point, primarily utilizing permanent magnetic force to suspend against gravitational input. When loads change or disturbances occur, the system generates current to maintain balance. All designs have passed validation. Experimental results demonstrate the improved zero-power performance and disturbance rejection capabilities of the proposed Maglev system. During synchronous operation, dynamic characteristics have shown significant improvement, which has been experimentally confirmed.

Keywords: Maglev system; state feedback control; zero-power control

check for updates

Citation: Tang, X.; Hashimoto, S.; Kawaguchi, T.; Kurita, N. Zero-Power Control Strategy and Dynamics Enhancement for Hybrid Maglev Conveyor Cart. *Electronics* **2024**, *13*, 2921. https://doi.org/10.3390/electronics13152921

Academic Editors: Ahmed Abu-Siada and Jianguo Zhu

Received: 17 May 2024
Revised: 15 July 2024
Accepted: 21 July 2024
Published: 24 July 2024

Copyright: © 2024 by the authors. Licensee MDPI, Basel, Switzerland. This article is an open access article distributed under the terms and conditions of the Creative Commons Attribution (CC BY) license (https://creativecommons.org/licenses/by/4.0/).

1. Introduction

Magnetic source devices produce a magnetic field that exerts both force and torque to propel a ferromagnetic object. Levitation may potentially be attained if the magnetic force balances the gravitational force acting on the object in question [1]. Traditionally, there was a distinct space between the magnetic source device and the ferromagnetic object [2,3]. Magnetic levitation (Maglev) technology enables the transfer of objects without physical touch, resulting in rapid movement and the elimination of vibrations. This advanced technology has been widely used in different industries, such as magnetically levitated trains, bearings, and high-speed lifts [4,5]. Magnetically levitated conveyor carts have been extensively utilized in several airports, providing benefits such as rapid speed, effectiveness, low noise, and energy preservation, significantly improving the efficiency of luggage transportation [6–8].

Various Maglev (magnetic levitation) systems have been used in the design of the transportation tools, such as wafers, optical lenses, electric vehicles, and transportation carts. According to the characteristics of magnetic levitation materials, there exist three primary types of ferromagnetic levitation systems: the electromagnet system (EMS), the permanent magnet system (PMS), and the hybrid electromagnet system (HEMS) [9–11]. In the EMS, levitation control relies on adjusting the input current of coils, enhancing response speed and mitigating control complexity. A steady-state current is employed to generate levitation force, leading to challenges such as coil heating and high energy consumption during continuous operation [12,13]. The PMS adjusts the magnetic force by manipulating the flux in the magnetic circuit, enabling reduced energy consumption due to the inherent magnetism of permanent magnets [14]. However, the PMS loses control if the levitated object comes into contact with the permanent magnet or magnet yoke. The HEMS

employs both permanent magnets and electromagnets to create a combined magnetic field. The electromagnet serves to enable active control, while the permanent magnet provides passive levitation stiffness.

To realize magnetic levitation and zero-power levitation, many researchers have investigated the control strategies for different hybrid EMSs. At the equilibrium position, the levitation force is solely generated by permanent magnets, necessitating an applied current of zero. The Korean research group of Kim et al. [15] studied another zero-power control method by combining a modified state feedback controller with voltage integration, eliminating the need for current measurement. Morishita et al. [16] proposed a zero-power control method that incorporated integral compensation into the conventional PID control system. This approach utilized integral current feedback and adjusted the reference air gap to attain zero current at the balanced state. Bozkurt et al. [17] integrated the control algorithm with the disturbance observer's forward feeding output and applied it to the HEM (hybrid electromagnet) flexible conveyor system. In [18], an extended Luenberger observer was employed for load sensing in the zero-power controller. The enhanced control method demonstrated excellent performance in experiments involving variable loads. In the realm of zero-power levitation research, various control strategies for different hybrid EMS systems were investigated. However, the equilibrium position's air gap varied based on the object's mass, necessitating system adjustments to ascertain the unique equilibrium position associated with zero-power levitation [19]. In an effort to reduce manufacturing costs, Wei Zhang et al. [20] combined the zero-power control method with sensor electromagnetic levitation, albeit at the expense of precise levitation positioning. The multi-pole Maglev system with zero-power has the problem of energy cost and the ease with which the limitation caused by various mass loads can be reached, which cannot be avoided in magnetic transportation applications.

This paper introduces an upgraded zero-power controller that improves the performance of conventional state feedback controllers. The mechanical model is in accordance with the prototype in [3]. In [3], a Maglev cart was successfully controlled by a PID controller. In this paper, the controller proposed here is controlled by the traditional state feedback controller. To eliminate steady-state errors, we include integral control for position, enhancing its resistance to interference. This effectively reduces external disturbances and minimizes steady-state errors, ensuring precise control. Next, to achieve the zero-power controller, we added the zero-power integral controller in the position servo control loop. When the zero-power controller is active, it allows the system to achieve equilibrium independently with magnetic force. We then conducted various load tests and demonstrated the effectiveness of the proposed Maglev system with the zero-power controller. Finally, the experiments with various loads on the four Maglev units working synchronously also proved their effectiveness.

The organization of this article is outlined as follows. Section 2 presents the design of key mechanical structures and their operational principles, as well as the establishment of the Maglev mathematical model. A zero-power controller is constructed in Section 3, utilizing the state feedback controller. Section 4 involves conducting simulations and levitation tests to validate the system's performance. Finally, Section 5 provides a conclusion to the essay and discusses the other tasks that need to be addressed.

2. Description of Maglev Conveyor System

2.1. Introduction of Maglev Conveyor System

A Maglev cart has four Maglev units in its system. To better describe the Maglev cart system, Figure 1 illustrates the detailed part of four units. The Maglev cart's mechanical design process and the the electromagnetic force analysis have been explored in the [3]. The parameters of the mechanical part and the electronics are kept in accordance with [3]. The coil wound around the PM unit was installed on the bottom of the bracket. The coil current is the control variable $i(t)$ of Maglev system unit. The eddy-current displacement sensor was installed on the top of bracket. The sensor detects the displacement of the rail

movement $x(t)$ in the vertical direction. The Maglev unit and the eddy current sensor were installed on the bracket. Moreover, there are touchdown wheels assembled on the bracket, which restricts each Maglev unit to only be able to move in vertical directions by ±1 mm. The left part of Figure 1 also indicates the 3D view of the Maglev cart system.

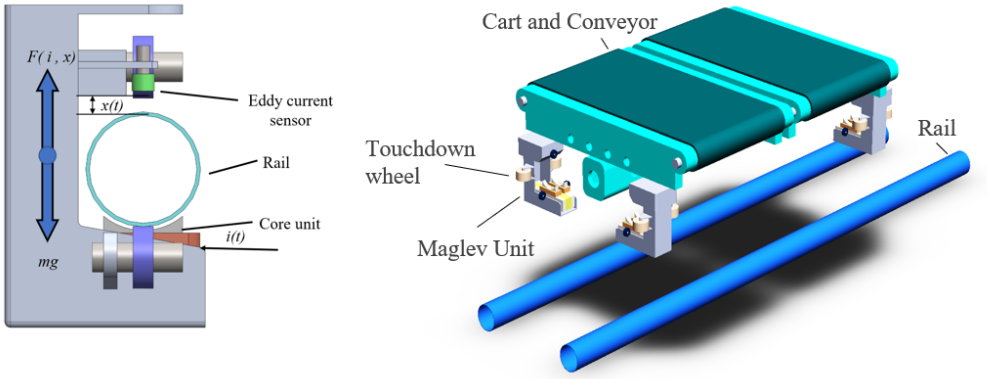


Figure 1. Force analysis of Maglev unit and 3D mechanical structure of the Maglev system.

2.2. Maglev Force Modelling

Constructing a model for the design of the control logic of a four-unit cart is important. However, when it comes to controlling the four-unit model, factors such as interference and slight deformations make precise control extremely challenging. Consequently, in this paper, for the simplicity of the control system design, we only focus on controlling each individual Maglev unit instead of the four-unit model for unified control. In order to construct a simple and reliable mathematical model of the Maglev unit cart system, some prerequisites need to be clarified. Magnetic flux leaks, edge effects, and the reluctance between the rail and the electromagnet are ignored [20]. The electromagnet unit is assumed to be a homogeneous sphere, and the magnetic force is concentrated at its center. There is assumed to be a linear relationship between the output current and input voltage of the power amplifier, with no delay.

To have a good understanding of the mathematical relationship of the Maglev system, the force analysis is shown in Figure 1. After the mathematical model of the system was analyzed, the mathematical relationship of the Maglev system is established through the following theoretical derivation from Newton's Second Law:

$$m\frac{d^2x(t)}{dt^2} = F(i,x) + mg \tag{1}$$

In Equation (1), m is the design quality in this project, g is the gravity acceleration, x is the ball balance position. $F(i,x)$ is the electromagnetic force on the magnetic unit, and i is the instantaneous current of the electromagnet winding. Based on the Kirchhoff Laws and Biot–Savart Law of the magnetic circuit, the electromagnetic force on the float unit is assumed as follows:

$$F(i,x) = -\frac{\mu_0 AN^2}{4}(\frac{i}{x})^2 \tag{2}$$

Here, we define $K_c = -\frac{\mu_0 AN^2}{4}$ as the constant coefficient related to the magnetic flux of the electromagnetic winding. When the ball is in equilibrium, the formula is obtained according to the mechanical balance principle as

$$mg + F(i_0, x_0) = 0 \tag{3}$$

in which i_0 and x_0 are the current and air gap (i.e., displacement) at the equilibrium point, respectively, and i_0, x_0 are the air gap and the current in the coil when the Maglev unit

maintains balance. Furthermore, the following relationship between position and current are at the equilibrium point can be obtained.

$$i_0 = \sqrt{\frac{-mg}{K_c}} x_0 \tag{4}$$

Obviously, Equation (1) had countless equilibrium positions, but some are unrealistic. Next, we linearize Equation (1) around the equilibrium point (i_0, x_0) as follows:

$$m\frac{d^2(\delta x(t))}{dt^2} = K_c \frac{i_0}{4x_0^2}\delta i(t) - K_c \frac{i_0^2}{4x_0^3}\delta x(t)) \tag{5}$$

where $\delta x(t) = x(t) - x_0$ and $\delta i(t) = i(t) - i_0$. Taking the Laplace transform, the linearized transfer function from $\delta i(t)$ to $\delta x(t)$ is

$$\delta x(s) = \frac{-k_i}{ms^2 - k_s}\delta i(s), \tag{6}$$

where $ki = -K_c \frac{i_0}{2x_0^2}$ and $k_s = -K_c \frac{i_0^2}{2x_0^3}$.

In this paper, we measure x_0 and i_0 at the selected equilibrium point; thus, we obtain the values of k_i and k_s as well. The specific values are shown in Table 1. It is worth noting that we only control the current increment δi, and i_0 is provided by an electromagnet with a constant current. Therefore, for controllers, there is a slight misuse of symbols without ambiguity, we directly use the symbol i to represent δi in the following.

Table 1. Nomenclature of physical parameters of the magnetic levitation unit.

Parameter	Description	Numerical Value
x^*	Target position	0 mm
x_0	Gap position	4 mm
i_0	Control current	0.05 A
μ_0	Vacuum permeability	$4\pi \times 10^{-7}$ (H/m)
A	Magnetic permeability area	$\pi \times 10^{-4}$ (m^2)
N	Coil turns	670
m	Suspend float	70 kg
k_i	Gain of current and the force	85 (N/A)
k_s	Gain of position and the force	1.5×10^5 (N/m)

Given that the Maglev system is highly regulated, which was proved in [3], the Maglev system can also be represented by a state space equation as Equation (7).

$$\begin{cases} \dot{x} = Ax + Bv \\ y = Cx + D \end{cases} \tag{7}$$

According the former analysis, the Maglev units system's kinematic model can be denoted as

$$\begin{cases} (k_i u + k_s x) \cdot \dfrac{1}{ms} = v \\ v \cdot \dfrac{1}{s} = x \end{cases} \tag{8}$$

According to the Maglev unit system's motion relationship and the relationship of current and velocity, we could obtain

$$\dot{x} = v \tag{9}$$

$$\dot{v} = \frac{k_i}{m}u + \frac{k_s}{m}x \tag{10}$$

x denotes displacement, v denotes velocity, u represent the voltage, m denotes mass, k_i denotes gain of current and the force, and k_s gain of position and force.

Taking the mathematical relationships above into consideration,

$$\begin{bmatrix} \dot{x_1} \\ \dot{x_2} \end{bmatrix} = \begin{bmatrix} 0 & 1 \\ \frac{k_s}{m} & 0 \end{bmatrix} \begin{bmatrix} x_1 \\ x_2 \end{bmatrix} + \begin{bmatrix} 0 \\ \frac{k_i}{m} \end{bmatrix} u \tag{11}$$

$$y = \begin{bmatrix} 1 & 0 \end{bmatrix} \begin{bmatrix} x_1 \\ x_2 \end{bmatrix} \tag{12}$$

In this equation we see that $A = \begin{bmatrix} 0 & 1 \\ \frac{k_s}{m} & 0 \end{bmatrix}$, $B = \begin{bmatrix} 0 \\ \frac{k_i}{m} \end{bmatrix}$, $C = \begin{bmatrix} 1 & 0 \end{bmatrix}$, and $D = [0]$.

To eliminate steady-state errors, as mentioned before, we need to introduce an integral item, that is, the augmented term x_a, which is satisfied as $\dot{x}_a(t) = x^* - x$, where x^* is the desired displacement. Thus, the state space equation of the augmented system is

$$\begin{aligned} \dot{x} &= A'x + B'u \\ y &= C'x + D' \end{aligned} \tag{13}$$

where $A' = \begin{bmatrix} A & 0 \\ -C & 0 \end{bmatrix}$, $B' = \begin{bmatrix} B^T & 0 \end{bmatrix}^T$, $C' = \begin{bmatrix} C & 0 \end{bmatrix}$ and $D' = [0]$.

3. Design of Maglev Unit Controller

3.1. Principle of Maglev Unit State Feedback Controller

In this approach, the Maglev system is designed by the pole placement methods of the root-loci, and the designed state feedback controllers capture all states and then multiply them by appropriate coefficients to generate the control signals. The stability of a system in classical control theory is influenced by the location of its poles. Moreover, the efficiency of a system is predominantly influenced by the arrangement of the poles. Therefore, by choosing a feedback gain matrix, we can achieve the necessary dynamic performance based on a given set of poles.

In this research, this method focuses on the analysis of the current amplifier and coil circuit operating in linear mode. The amplifier k_{amp} is presented in the system. For the coil unit, which requires strict and high-precision control, we introduce a position servo integrator to eliminate steady-state error in the balanced position. The position servo integrator is placed in combination with the feedback controller to eliminate steady-state errors [21]. The original Maglev system is a typical second order system. Hence, the system's order is increased to three. Three-order poles, based on the pole placement theory, are placed in the left half plane (LHP). There are three feedback gain parameters: one for the displacement of the system output, denoted as f_x; one for velocity, denoted as f_v, which is difficult to measure directly (here, we derive it by using an approximate derivative of position as a replacement for velocity detection); the final parameter is denoted as f_{sv}. This part is shown in Figure 2, Region 2.

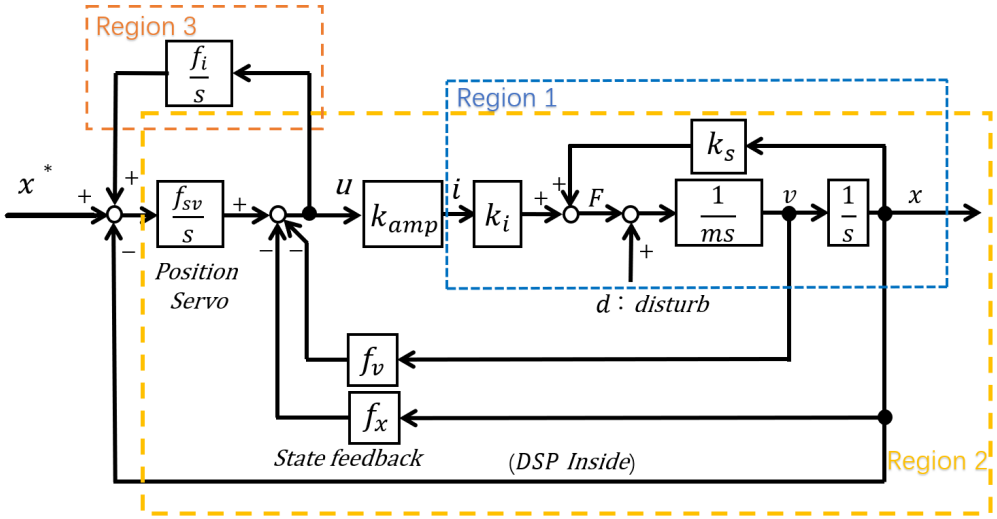


Figure 2. The overall system block diagram based on the state feedback controller that integrates position servo and zero-power control.

3.2. State Feedback Controller Designed with Zero-Power Control

The state feedback controller is designed with pole placement theory in the Maglev unit system. The system balance condition is that the poles of the system transfer function in the Laplace domain should be located in LHP. It is obvious that the poles in Equation (6) are not in the LHP. Therefore, the state feedback controller based on pole placement is designed as Equation (14):

$$u = F_1 x \tag{14}$$

The negative notation in (14) shows that signal feedback to the system was negative. The parameters F_1 are a gain vector, and x is a state quantity. Hence,

$$F_1 = [f_x, f_v, f_{sv}] \tag{15}$$

The closed-loop state space equation with the state feedback controller shows:

$$\begin{aligned} \dot{x} &= (A' - B'F_1)x \\ y &= C'x \end{aligned} \tag{16}$$

Before design the controller for the new gain matrix system, the controllability of the gain matrix must be determined. The determine process show as:

$$\text{rank}[B, AB, A^{n-1}B] = q \tag{17}$$

Hence, the closed-loop transfer function is changed to an autonomous system. The stability of the closed-loop system is based on the matrix $(A - BF_1)x$ eigenvalue. The real parts of the eigenvalues are all strictly negative whilst the system is stable. In the calculation of the controllers K, we obtain the characteristic equation

$$\det|sI - (A - BF_1)| = 0 \tag{18}$$

The configured closed-loop system also has an s descending power arrangement characteristic equation, which we set as

$$|sI - (A - BK)| = (s - s_1)(s - s_2)(s - s_3) \cdots (s - s_n) = 0 \quad (19)$$

Figure 2 illustrates the whole diagram of the proposed controller integrated in the Maglev system. In the state feedback controller of the Maglev unit system, the $rank = 3$, which corresponds to the length of the matrix $(A - BF_1)$ [21]. Therefore, all the states of the Maglev unit are controllable. Based on the three multiple poles in the Maglev unit controller, the three multiple poles are set on -20. With the help of MATLAB 2022a calculations, the parameters of the controller are $f_x = 1.7$, $f_v = 0.02$, $f_{sv} = 2.1$, which is presented in $F_1 = [f_x, f_v, f_{sv}]$. The guideline for pole placement should be as close to the stroke limit as possible, with no overshoot, and with fast settling time and stability. Hence, the pole placement was set on the real axis, the adjustment of which was determined through trial and error by experiment. In the simulation, there are three series poles, -10, -20, -30, that were tried; this was clearly stated in the Section 4.3: Unique Maglev System Levitation Experimental Results.

There are several zero-power control methods available, such as using an observer, a current integral feedback, or object weight estimation. In this paper, we consider a controller with simple integration. The state feedback controller with commonly used current integral feedback leads to the state feedback equation. Using this method, the last integral term will have a constant value after convergence, and the steady current approaches zero [15]. Here, f_i is a positive gain that determines the speed of convergence. The gain f_i can be selected independently of the pole placement. The equation can be modified to use voltage feedback instead of current feedback. Similarly, the voltage approaches zero after convergence, and the current also goes to zero. With this modification, current measurement is not necessary [15]. This part is shown in Figure 2, Region 3. The zero-power controller is based on a state feedback controller, where f_i/s is used as an integrator to eliminate static errors in response to step disturbance inputs. Here, f_i is an experimental parameter with a value of 1 in this zero-power control loop. The parameter f_i can be obtained by two methods: by calculation or by the trails in the experiment, which is feasible. In this experiment, the parameter was obtained by the latter one. The f_i was set at 0 and gradually increased, and the control performance reached its optimum at a value of 1. Beyond this point, the control effectiveness deteriorates. In the controller logic diagram, the input of the control is the final displacement of each unit. The control force was generated by the coil magnetic force, which is indicated in Figure 2. All parameters and the control logic circuit are embedded in the dSPACE control logic circuit. The feedback current is internally calculated in the dSPACE.

4. Experimental Result and Test Analysis

4.1. Maglev System Integration

The experimental prototype of the Maglev unit system is shown in Figure 3. The electrical processing circuit used with the controller is designed to keep the system stable. The electrical processing circuit consists of the DSP, current amplifier, sensor measurement circuit, and coil. The power supply selected is CME-A350-24V(TDK), which supplies 24 V voltage for system operation. The eddy current sensor is model 7620-146(AEC). It has a measurement range of $\pm$10 mm, a resolution of 2 µm, and a linearity of $\pm$1% (0.7–6.3 mm). The current amplifier is the Copley_4122Z_EN DC brush servo amplifier (Copley Controls). It has a 3 kHz bandwidth, and the wide load inductance is 0.4–40 mH. The DSP used in this experiment is the dSPACE DS1104. The dSPACE real-time simulation system is a MATLAB/Simulink 2022a control system development and testing work platform.

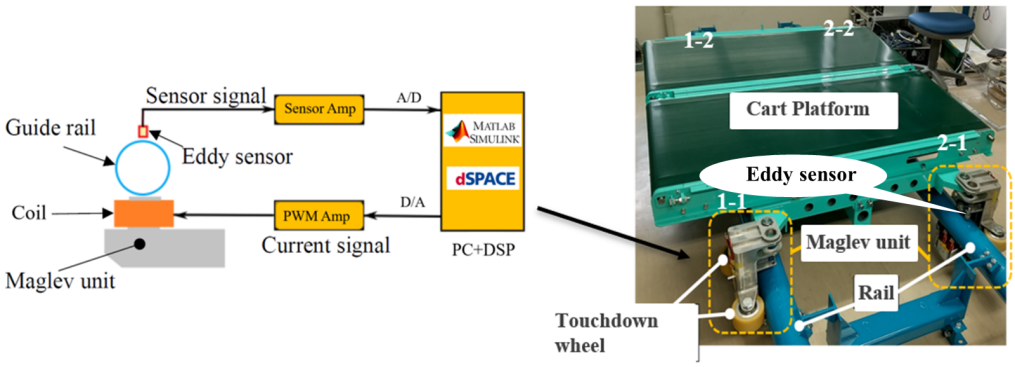


Figure 3. Maglev unit electrical control logic circuit with MATLAB/Simulink and dSPACE. In Maglev cart, the four Maglev Unit are marked with the serial number: Unit 1-1, Unit 1-2, Unit 2-1 and Unit 2-2.

4.2. Maglev System Simulation

The simulation results are displayed in Figure 4. The system's effectiveness is tested by implementing the state feedback controller and assessing the impact of the ideas. During the simulation, we conducted an analysis by comparing three multiple poles at -10, -20, and -30. When the three multiple poles were at -10, the controller parameters of the $F_1 = [f_x, f_v, f_{sv}]$ were $f_x = 1.3, f_v = 0.01, f_{sv} = 0.3$; when the three multiple poles were set at -20, the controller parameters of the $F_1 = [f_x, f_v, f_{sv}]$ were $f_x = 1.7, f_v = 0.02, f_{sv} = 2.1$; when the three multiple poles were at -30, the controller parameters of the $F_1 = [f_x, f_v, f_{sv}]$ were $f_x = 2.2, f_v = 0.03, f_{sv} = 8.4$. The parameters of the controller are calculated with the same method of the controller design idea that was presented in the Section 3.2. After obtaining the controller parameters, we built the Matlab/simulik simulation logic system. The simulation results are clearly explained in our design ideas. Frequency domain-analyzed results and time domain-analyzed results were obtained. The frequency results in Figure 4a indicate that the system with a zero-power controller performed well. The low-frequency band is horizontal and the gain decreases high-frequency band. The rising speed is from slow to fast, consistent with the multiple poles of -10, -20, -30. In the time domain of Figure 4b, at time 0 s, the status feedback controller is engaged, leading to the accurate tracking of a displacement of 1 millimetre. At 3 s, the zero current controller is engaged to prevent any steady-state current or positional deviation in the system. At 7 s, a 8 kgf disturbance is applied, resulting in a shift in the equilibrium position of the system due to changes in weight.

Simultaneously, when examining the current of the system, we noticed a sizable transient current at 3 s. With the activation of the zero current controller, the current gradually approached 0 A. Following the introduction of the disturbance, transient current was initially generated, but eventually, the system's current remained at 0 A.

4.3. Unique Maglev System Levitation Experimental Results

The simulation results agreed well with the design concept. The controller of the Simulink block diagram was implemented into the dSPACE. The different controllers' parameters in the actual experiment were kept in accordance with the parameters that have been presented in the simulation section. In the experiment, we tried three multiple poles. The experimental results were not as ideal as the simulation. The experimental equipment have the boundaries and limitation of the calculation. Figure 5 illustrates the performance of the state feedback controller design with different multiple poles. In the experiments, the three multiple poles at -10 were too slow to support the levitation. When the multiple poles were set at -20, the controller had an excellent control performance. However, when the multiple poles were set at -30, the response of the controller was too fast, which generated a high amount of high-frequency vibrations. Based on the trial and error principle, considering the response speed and stability margin, we chose the multiple poles at -20 as the system controller parameters.

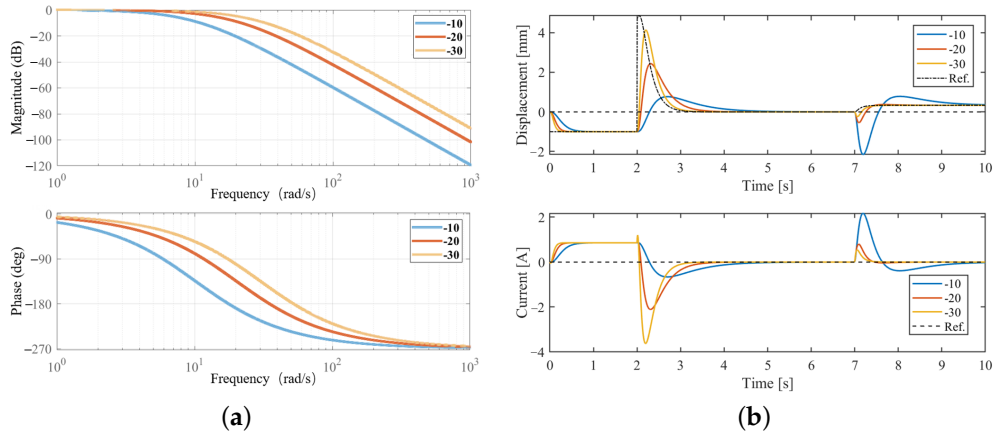


Figure 4. Simulation results of Maglev unit with zero-power controller in MATLAB with different poles. (**a**) Magnitude and phase of unique Maglev unit's simulation ; (**b**) Displacement and current of unique Maglev unit's simulation.

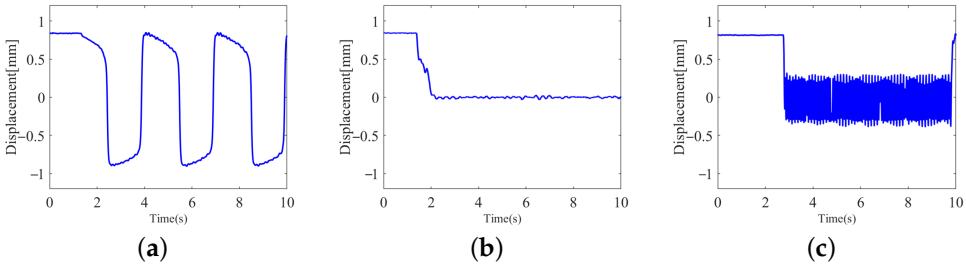


Figure 5. Experimental results of state feedback controller with multiple poles of -10, -20, -30. (**a**) Multiple poles of -10; (**b**) Multiple poles of -20; (**c**) Multiple poles of -30.

Figure 6a illustrates the outcome of the displacement and current of the Maglev unit, which is regulated by the state feedback controller without the zero-power controller. Upon activating the state controller, the system exhibits consistent positioning at 0 mm, accompanied by a current of around -0.2 A, hence guaranteeing the stability of the system at the 0 mm position. Approximately 12 s later, an 8 kgf perturbation is introduced, and it is found that the system rapidly returns to the 0 mm position. Furthermore, the system's current undergoes variations, resulting in a consistent output of $+0.2$ A.

Figure 6b displays the experimental results of displacement and current for the Maglev unit, which was controlled by a state feedback controller with a zero-power controller. The status feedback controller is engaged prior to 0 s, and the system maintains stability. The zero current controller is activated at around 3 s. Over time, it is noticed that the system's current gradually approaches zero, while the equilibrium position gradually moves away from 0 mm and settles at a new equilibrium point. At around 14 s, an 8 kgf disturbance is added, resulting in a temporary alteration in the current. After approximately 1 s, the current recovers to a value of 0 A. At the same time, the reference position also undergoes automatic changes, ultimately reaching a stable state at a different equilibrium point. Consequently, the distinctive Maglev unit method attains genuine levitation with zero current.

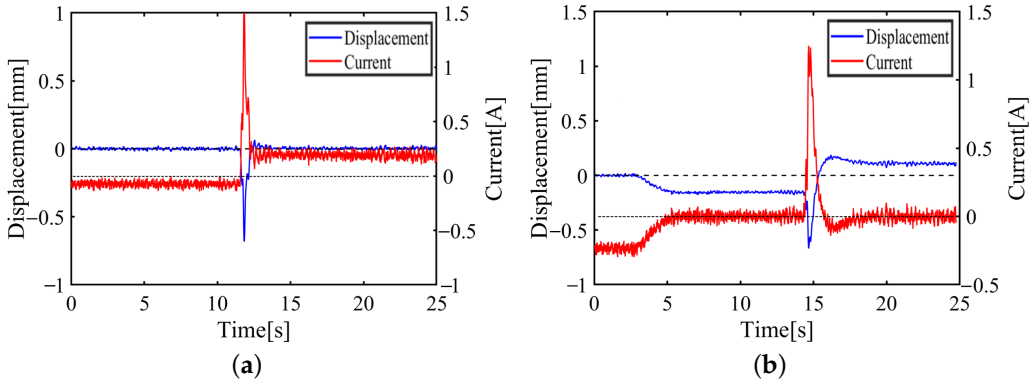


Figure 6. Experimental result of displacement and current of Maglev unit controlled by state feedback controller combined with and without zero-power control. The dot line in the Figure indicated the reference line for 0 mm and 0 A. (**a**) States feedback controller; (**b**) Zero-power controller.

Furthermore, to verify the controller's performance and stability, different load tests were conducted under the control of the SFB controller with and without a zero-power controller. The current consumption and the displacement movement of the steady-state results are summarized in Table 2. Declaration: The weights used for testing were solid-state batteries. The test results are records based on actual experiments.

Table 2. The steady-state current and displacement under the force loads for SFB controller and SFB controller with zero-power controller.

Loads of Baggage	Current in SFB Controller	Displacement in SFB Controller	Current in SFB and Zero-Power Controllers	Displacement in SFB and Zero-Power Controllers
8 kgf	−0.8 A	0 mm	0 A	−0.7 mm
16 kgf	−0.7 A	0mm	0 A	−0.5 mm
24 kgf	−0.4 A	0 mm	0 A	−0.25 mm
32 kgf	−0.3 A	0 mm	0 A	−0.18 mm
40 kgf	−0.18 A	0 mm	0 A	−0.07 mm
48 kgf	−0.25 A	0 mm	0 A	−0.15 mm

In the evaluation process of energy consumption, which is mainly caused by the copper coils, we calculate the integral of instantaneous thermal power versus time within 1 s of the stable levitation state. Then, the total energy consumption of the Maglev system corresponding to levitation time T is obtained, as shown in Equation (20).

$$Q_c = \frac{1}{t}\int_T^{T+t} i^2 Ri(t)d(t) \tag{20}$$

The energy consumption of the Maglev system, when combined with the zero-power controller of the SFB controller, is significantly lower compared to when the system is managed only by the SFB controller. When the Maglev unit work in steady state and the Maglev unit levitated a 30 kgf load, the Maglev system controlled by the state feebback controller without a zero-power controller consumes roughly 0.96 J per second. The 30 kgf is to simulate actual luggage weight.Therefore, at the same experimental condition, the energy consumption of the state feedback controller with zero power will be reduced to about 0.1 J per second. Energy usage is greatly reduced while using the proposed state feedback controller with the zero-power controller.

The design of the Maglev unit in this study potentially meets the design standards. The Maglev unit is equipped with a zero-power controller that enables the detection of a new equilibrium position when the controller is activated.

4.4. Maglev System Levitation Experimental Results

As depicted in Figure 3, a single cart platform was suspended using four Maglev units that were mounted on the cantilever bracket. The ultimate objective of the Maglev cart's control system is to ensure that all four Maglev units operate in perfect synchronization to achieve the levitation of the object.

There are four Maglev units that are installed on the four corners of the cart. The two Maglev units in the neighbourhood cause disturbances, because the two Maglev units have a horizontal long-side distance of 1800 mm and a horizontal short-side distance of 1050 mm. The loads weigh more than 70 kg, including the cart. In modeling, it is generally assumed that the weight of an item is maintained by the combined action of four points. The overall weight of the object is equal to the sum of the weight supported by these four points of the cart. The issue of coupling and mutual influence was determined to be insignificant during the experimental procedure. For the simplified model set-up, the decoupling question is not explored here.

Before conducting the experiment, several pre-conditions were set. The state feedback controller parameters of four Maglev units were set as follows: $F_1 = [-1.7, -0.02, -2.1]$. The zero-power controller parameters were set as $f_i = 1$. There are three experimental text scenarios: static levitation, dynamic levitation disturbances input. All the situations are shown as follows. The experimental tests' pre-condition is that the four Maglev units work in the steady state. All experiments were conducted under identical conditions. For the three scenarios test, the judgment criteria of the four Maglev units are stated here. The move range of each unit in the vertical direction was ± 1 mm, and each unit working in the displacement range -1 mm–$+1$ mm indicated that the unit was in a steady state. Four Maglev units being levitated by the electromagnetic force in the range without touching the rail meets the control target. In here, the four units being in the same displacement is not a mandatory conditions. In the test scenarios, we also designed one unit to levitate greater loads, which more clearly showed the changes in the Magelv units under the controller of the stated feedback controller with and without the zero-power controller. There was no working limitation on the current. Under the controller of the state feedback without the zero-power controller, the Maglev units had the same displacement, but the current cost of each Maglev unit was not the same. The current was influenced by the loads. The Maglev units were controlled by the state feedback controller with a zero-power controller, the four Maglev units cost nearly 0 A current, their displacement was not same. The displacement was influenced by the loads.

4.4.1. Scenario 1: Static Levitation

Scenario 1 (static levitation) interpretation: The four units of the cart were levitated at the equilibrium position with a 30 kg load on the cart platform. The cart remained static without any horizontal movement. Initially, the state feedback controllers were activated one by one, and then the displacement and current of each Maglev unit were measured. These data are illustrated in Figure 7a for the time zone from 0 s to 26 s. Subsequently, the zero-power controller began operating simultaneously with the state feedback controller. This resulted in changes in displacement and current, with each Maglev unit reaching a new equilibrium point. The results for the time zone from 26 s to 60 s are depicted in the Figure 7a. Under the control of the state feedback controller with the zero-power controller, the displacement of each Maglev unit did not remain at 0 mm. The coil current of the four Maglev units remained nearly 0 A. Thus, the static levitation scenario successfully demonstrated zero-power control.

4.4.2. Scenario 2: Dynamic Levitation

Similar to the static levitation scenario, a 30 kg load was placed on the cart platform. The cart started with the controllers turned off. In scenario 2, the cart not only remained levitated at the equilibrium point but also moved in the horizontal direction. First, the state feedback controllers were turned on one by one, allowing the cart to levitate in a static state. Once the cart stabilized, it moved forward horizontally at a speed of 0.2 m/s. Under the control of the state feedback controller without the zero-power controller, the displacement and current of the four Maglev units were recorded, as shown in Figure 7b. From 0 to 26 s, the Maglev cart was controlled by the state feedback controller without the zero-power controller. During this period, the displacement of the four Maglev units remained at 0 mm. To balance the load force, the currents in the coils of the four Maglev units were not zero. Specifically, the current in unit 2-2 was maintained at 0.7 A. Subsequently, the zero-power controller was activated. From 27 s to the end of the observation period, under the control of the state feedback controller with the zero-power controller, the displacements of the four Maglev units did not stay at 0 mm but balanced at a new equilibrium point. The currents in the Maglev units were maintained at 0 A. The experimental results are consistent with the static control scenario. The four Maglev units were able to levitate the cart under the control of the state feedback controller both with and without the zero-power controller.

Accordingly, the Maglev cart levitated the nominal weight at the equilibrium working point, both in static and dynamic settings. Nevertheless, vibrations were more noticeable under dynamic settings in contrast to static ones. The system effectively maintained the equilibrium point at 0 mm under the control of the four state feedback controllers. When the Maglev system was controlled by the state feedback controller combined with the zero-power controller, it functioned at the equilibrium point, resulting in a reduction in the current consumption to nearby 0 A.

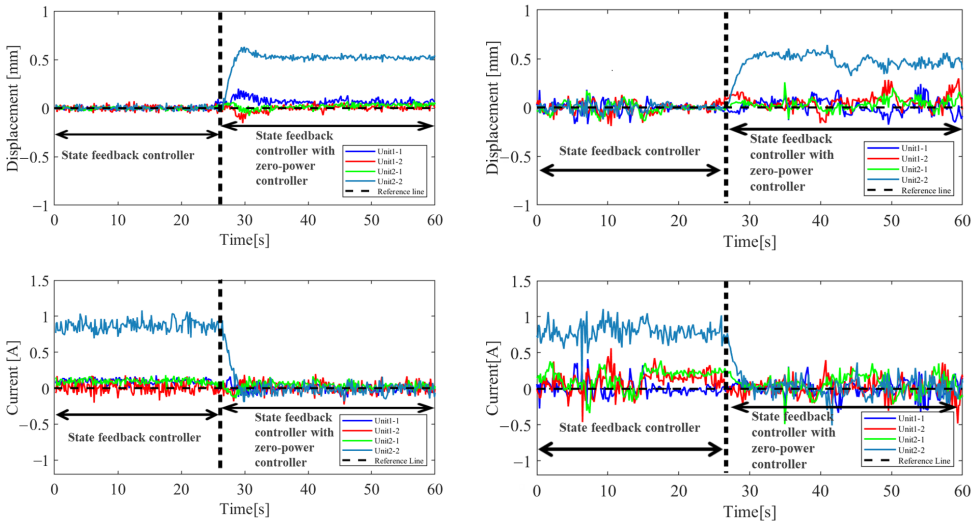


Figure 7. Experimental result of displacement and current of four Maglev units working synchronously with state feedback controller combined with zero-power control. (**a**) Scenario 1: displacement and current output in static; (**b**) Scenario 2: displacement and current output in dynamic.

4.4.3. Scenario 3: Disturbance Input

The disturbance input scenario involved the cart being levitated by four Maglev units. Initially, the cart was levitated by the four Maglev units, which were controlled by a state feedback controller without a zero-power controller, and were in a static state. The displacement and current of the four Maglev units began to be recorded, as shown in Figure 8. At approximately 10 s, a 10 kgf load was added to the Maglev cart. This disturbance generated some small currents to resist the disturbance and caused some

displacement changes, as illustrated in the disturbance input part of Figure 8. At 40 s, the 10 kgf disturbance was removed, and the four Maglev units returned to their original state. At 55 s, the zero-power controller was activated, and the cart continued to move along the rail. Within the next 5 s, the four Maglev units reached a steady state. Then, the same 10 kgf load was added to the cart again, causing oscillations in the Maglev units. The units generated currents to counteract these oscillations, although some oscillations persisted. At 130 s, the 10 kgf disturbance was removed, and the four Maglev units of the cart recovered to the balanced state after the disturbance was removed. A total of 10 s later, the Maglev system was completely turned off. In this scenario, the four Maglev unit experimental results were in accordance with the former two scenarios. Regarding the disturbance, both controllers have a strong anti-interference capability.

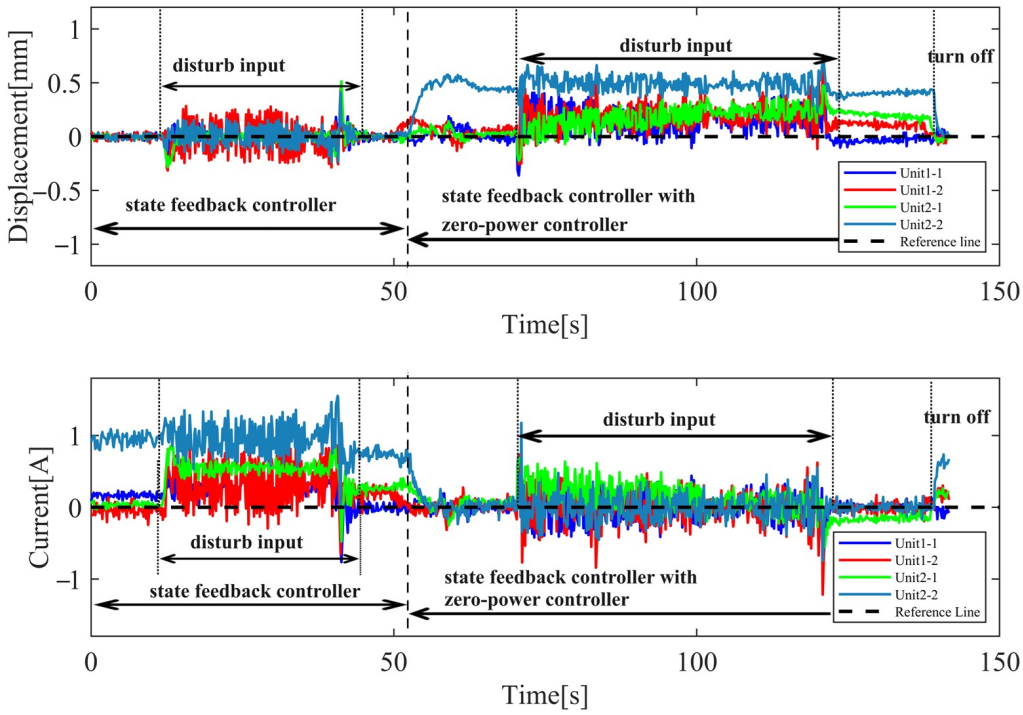


Figure 8. Scenario 3: Experimental result of displacement and current, tested under the condition of a 10 kg input of 4 Maglev units working synchronously with a state feedback controller combined with zero-power control.

After multiple scenarios had been tested, both the state feedback controller and its integration with the zero-power controller could achieved the cart work at the equilibrium position. Upon comparing the two controller, it was found that the state feedback controller demonstrated superior anti-interference capabilities, whilst the integration with the zero-power controller exhibited exceptional power-saving capabilities. Both controllers meet the design expectation. According to Equation (20), the Maglev system working under the control of the state feedback controller without a zero-power controller will cost 1.2 J per second. The Maglev controller working under the controller of the state feedback controller with the zero-power controller only cost about 0.2 J per second. In the long-term working condition, the zero-power controller will save a lot energy. For the better synchronization control of the Maglev cart, we need to control the four target positions, taking into account the geometry of the transport device. For that case design, calibration of position information (sensor and actuator placement) is also important. Moreover, this proposed method only focuses on zero-power control in addition to improving dynamic characteristics. A platform was needed for the three points. Hence, only position control at three zero-power points and proportional control at one point were used in the design in this project, and synchronization was not considered. Also, in [3], the three zero-power

control of position control and one-point proportional control were not achieved. So, the simple method for synchronization is to synchronize what controls the four Maglev units themselves.

5. Conclusions and Future Work

The article presented a Maglev prototype transportation cart that can achieve zero-power control with various mass loads. The proposed zero-power controller integrated a state feedback controller with a position servo. The position servo integrator in the controller was adjusted via pole placement to meet disturbance rejection and zero-power control requirements. A controller with disturbance rejection capability was designed to effectively manage an increasing current with a load while maintaining the desired levitation position. Furthermore, a zero-power controller was devised based on the state feedback controller, gradually transitioning the system to zero-power operation and adjusting equilibrium position with object gravity. Experimental results indicate that the Maglev unit system, employing the designed control algorithm, exhibited superior zero-power and disturbance rejection performance under varying eccentric load conditions. Efforts to develop a cooperative work strategy for multiple Maglev units and enhance system anti-disturbance capabilities in dynamic scenarios are also affirmed. The proposed method has two advantages: the improvement of dynamic characteristics and high-efficiency control, which can be achieved at the same time. The two controls can be designed separately, which provides good design visibility. By turning the zero-power control on and off, it is possible to switch between position control regarding stroke limitation and zero-power control focusing on high efficiency.

The expansion of the Maglev prototype into a multi-input and multi-output system will be used to re-create a math model to compare it with the current one. In the future, we will investigate the resilience and robustness performance under dynamic load based on the principle of [22,23], developing a nonlinear control algorithm, and improving positioning accuracy control. And also, we will explore the working applications that combine it with a linear driver in the horizontal movement.

Author Contributions: Formal analysis, S.H.; Data curation, T.K.; Writing—original draft, X.T.; Visualization, N.K. All authors have read and agreed to the published version of the manuscript.

Funding: This research received no external funding.

Institutional Review Board Statement: Not applicable.

Informed Consent Statement: Not applicable.

Data Availability Statement: Data are contained within the article.

Conflicts of Interest: The authors declare no conflicts of interest.

Abbreviations

The following abbreviations are used in this manuscript:

Maglev	Magnetic levitation
EMS	Electromagnetic system
PMS	Permanent magnet system
HEMS	Hybrid electromagnet system
PM	Permanent magnet
LHP	Left half plane

References

1. Tang, X.; Ishii, F.; Kawaguchi, T.; Hashimoto, S.; Kurita, N.; Hishinuma, N.; Egura, K.; Miyamoto, F. Design of Low-Power Consumption of Magnetic Levitate Transportation Unit Based on State Feedback Controller. In Proceedings of the IECON 2023-49th Annual Conference of the IEEE Industrial Electronics Society, Singapore, 16 October 2023; pp. 1–5. [CrossRef]
2. Qin, Y.; Yang, J.; Guo, H.; Wang, Y. Fuzzy Linear Active Disturbance Rejection Control Method for Permanent Magnet Electromagnetic Hybrid Suspension Platform. *Appl. Sci.* **2023**, *13*, 2631. [CrossRef]
3. Tang, X.; Hashimoto, S.; Kurita, N.; Kawaguchi, T.; Ogiwara, E.; Hishinuma, N.; Egura, K. Development of a Conveyor Cart with Magnetic Levitation Mechanism Based on Multi Control Strategies. *Appl. Sci.* **2023**, *13*, 10846. [CrossRef]
4. Zhai, M.; Long, Z.; Li, X. A new strategy for improving the tracking performance of magnetic levitation system in maglev train. *Symmetry* **2019**, *11*, 1053. [CrossRef]
5. Sun, F.; Oka, K. Zero power non-contact suspension system with permanent magnet motion feedback. *J. Syst. Des. Dyn.* **2009**, *3*, 627–638. [CrossRef]
6. Hu, K.; Jiang, H.; Zhu, Q.; Qian, W.; Yang, J. Magnetic Levitation Belt Conveyor Control System Based on Multi-Sensor Fusion. *Appl. Sci.* **2023**, *13*, 7513. [CrossRef]
7. Sun, Y.G.; Xie, S.; Xu, J.Q.; Lin, G.B. A Robust Levitation Control of Maglev Vehicles Subject to Time Delay and Disturbances: Design and Hardware Experimentation. *Appl. Sci.* **2020**, *10*, 1179. [CrossRef]
8. Zhao, C.; Oka, K.; Sun, F.; Harada, A.; Jin, J.; Zhang, M. Design of Zero-Power Control Strategy With Resisting Tilt of Hybrid Magnetic Levitation System. *IEEE Trans. Ind. Electron.* **2022**, *69*, 11394–11402. [CrossRef]
9. Ogiwara, E.; Kuirta, N.; Wang, B. Implementation and suspension force evaluation of a permanent magnet hybrid type magnetically levitated carrier system. *Dyn. Des. Conf.* **2021**, *2021*, 538. [CrossRef]
10. Kurita, N.; Hishmuma, N.; Egura, K. Development of Magnetic Levitation Conveyor with Permanent Magnet. *Dyn. Des. Conf.* **2019**, *2019*, 521.
11. Pourkand, A.; Abbott, J.J. Magnetic actuation with stationary electromagnets considering power and temperature constraints. *IEEE Robot. Autom. Lett.* **2020**, *5*, 6964–6971. [CrossRef]
12. Matsumoto, S.; Arai, Y.; Nakagawa, T. Noncontact levitation and conveyance characteristics of a very thin steel plate magnetically levitated by a LIM-driven cart. *IEEE Trans. Magn.* **2014**, *50*, 1–4.
13. Zhang, H.; Kou, B.; Zhou, Y. Analysis and design of a novel magnetic levitation gravity compensator with low passive force variation in a large vertical displacement. *IEEE Trans. Ind. Electron.* **2019**, *67*, 4797–4805. [CrossRef]
14. Zhao, C.; Sun, F.; Jin, J.; Tang, J.; Xu, F.; Li, Q.; Oka, K. Analysis of quasi-zero power characteristic for a permanent magnetic levitation system with a variable flux path control mechanism. *IEEE/ASME Trans. Mechatron.* **2020**, *26*, 437–447. [CrossRef]
15. Kim, C.H.; Cho, H.W.; Lee, J.M.; Han, H.S.; Kim, B.S.; Kim, D.S. Zero-power control of magnetic levitation vehicles with permanent magnets. In Proceedings of the ICCAS 2010, Gyeonggi-do, Republic of Korea, 27–30 October 2010; pp. 732–735.
16. Morishita, M.; Azukizawa, T.; Kanda, S.; Tamura, N.; Yokoyama, T. A new maglev system for magnetically levitated carrier system. *IEEE Trans. Veh. Technol.* **1989**, *38*, 230–236. [CrossRef]
17. Bozkurt, A.F.; Erkan, K.; Güney, Ö.F. Zero power control of a 3 dof levitated multiple hybrid electromagnet flexible conveyor system. In Proceedings of the 2015 Intl Aegean Conference on Electrical Machines & Power Electronics (ACEMP), 2015 Intl Conference on Optimization of Electrical & Electronic Equipment (OPTIM) & 2015 Intl Symposium on Advanced Electromechanical Motion Systems (ELECTROMOTION), Side, Turkey, 2–4 September 2015; pp. 570–575.
18. Kim, Y.H.; Kim, K.M.; Lee, J. Zero power control with load observer in controlled-PM levitation. *IEEE Trans. Magn.* **2001**, *37*, 2851–2854.
19. Mizuno, T.; Sakurada, T.; Ishino, Y.; Takasaki, M. Zero-power control of parallel magnetic suspension systems. *J. Syst. Des. Dyn.* **2011**, *5*, 765–776. [CrossRef]
20. Wei, Z.; Huang, Z.; Zhu, J. Position control of magnetic levitation ball based on an improved adagrad algorithm and deep neural network feedforward compensation control. *Math. Probl. Eng.* **2020**, *2020*, 8935423.
21. Sazawa, M.; Ohishi, K.; Katsura, S. High speed positioning servo system using integrator correction of PI controller based on disturbance observer. In Proceedings of the 2008 34th Annual Conference of IEEE Industrial Electronics, Orlando, FL, USA, 10–13 November 2008; pp. 2539–2544.
22. Zhang, W.; van Luttervelt, C. Toward a resilient manufacturing system. *CIRP Ann.* **2011**, *60*, 469–472.
23. Zhang, T.; Zhang, W.; Gupta, M.M. Resilient Robots: Concept, Review, and Future Directions. *Robotics* **2017**, *6*, 22. [CrossRef]

Disclaimer/Publisher's Note: The statements, opinions and data contained in all publications are solely those of the individual author(s) and contributor(s) and not of MDPI and/or the editor(s). MDPI and/or the editor(s) disclaim responsibility for any injury to people or property resulting from any ideas, methods, instructions or products referred to in the content.